PAPER

Check for updates

Rh single-atom nanozymes for efficient ascorbic acid oxidation and detection†

Xiaoyue Shi,[a,d] Juan Li,[a] Yu Xiong, ID *[b] Ziyu Liu,*[c] Jinhua Zhan ID [a] and Bin Cai ID *[a]

The management of ascorbic acid (AA) in biological fluids is of significant importance for body functions and human health, yet challenging due to the lack of high-performance sensing catalysts. Herein, we report the design of Rh single-atom nanozymes (Rh SAzymes) by mimicking the active sites of ascorbate peroxidase toward efficient electrocatalytic oxidation and detection of AA. Benefiting from the enzyme-mimicking single-atom coordination, the Rh SAzyme exhibits an unprecedented electrocatalytic activity for AA oxidation with an onset potential as low as 0.02 V (*vs.* Ag/AgCl). Combined with the screen-printing technology, a miniaturized Rh SAzyme biosensor was firstly constructed for tracking dynamic trends of AA in the human subject and detecting AA content in nutritional products. The as-prepared biosensor exhibits excellent detection performances with a wide linear range of 10.0 μM–53.1 mM, a low detection limit of 0.26 μM, and a long stability of 28 days. This work opens a door for the design of artificial single-atom electrocatalysts to mimic natural enzymes and their subsequent application in biosensors.

Introduction

Ascorbic acid (AA) plays an essential role in the maintenance of various health-determining substances, including collagen, carnitine, and neurotransmitters, thus representing one of the most common and effective nutrition supplements.[1] Moreover, the latest studies have revealed that AA plays a unique role in the prevention and treatment of COVID-19 and other similar coronaviruses.[2] Thus, maintaining a balanced AA level in the human body is essential to support physical and mental resilience.[3,4] To this end, tremendous research and commercialization efforts have been devoted to developing novel biosensors to continuously monitor personalized health status.[5–8] Among them, non-enzymatic electrochemical sensors have attracted immense attention due to their rapid, noninvasive, and miniaturization features. Their sensing performances are strongly dependent on the selectivity and activity of the electrocatalytic AA oxidation reaction. Due to the lack of high-performance electrocatalysts, however, further developments and practi-

cal applications remain a significant challenge.[9–11] Furthermore, the realization of efficient redox processes of AA in electrochemistry is highly desirable in the elucidation of its physiological and pharmacological action, the mechanism of which has been the subject of debate for decades.[12]

Single-atom catalysts (SACs) with enzyme-mimicking structures have emerged as a new frontier in the field of catalysis and hold promise to mimic ascorbate peroxidase.[13–21] Unlike the conventional nanocatalysts, SACs possess the active metals in a single-atomic scale, thus facilitating the exposure of active sites and promoting atom-utilization efficiency.[10,22–25] In addition, the active sites of SACs usually exhibit uniform geometric environments, which differ from those of the conventional nanocatalysts with diverse active sites (*i.e.* facets), thus leading to similar adsorption states to reaction intermediates and high selectivity. Recently, SACs have exhibited significant potential in various catalytic reactions, such as the ORR,[26,27] water splitting,[28,29] CO$_2$ reduction,[15,30] and nitrate reduction.[16,17,31] However, few studies have been reported on the design of SAC-based electrochemical sensors.[32–34] Furthermore, the active site of natural ascorbate peroxidase has been characterized as a central iron ion coordinated by the four pyrrole nitrogen atoms,[35,36] yet the design of SACs to mimic such structures with desirable activity remains a significant challenge.

Herein, we demonstrate the design of Rh single-atom nanozymes (Rh SAzymes), based on which a non-enzymatic electrochemical sensing platform has been developed. Rh is selected as the metal center due to its high electronegativity, which is beneficial for oxidative reactions, particularly dehydrogenation.[37] Combined with screen printing technology, miniaturized Rh

[a] *School of Chemistry and Chemical Engineering, Shandong University, 250100 Jinan, China. E-mail: bin.cai@sdu.edu.cn*
[b] *Department of Chemistry and Chemical Engineering, Central South University, 410083 Changsha, China. E-mail: thomas153@126.com*
[c] *Centre for Health Management and Policy Research, School of Public Health, Cheeloo College of Medicine, NHC Key Lab of Health Economics and Policy Research, Shandong University, Jinan, 250012, China. E-mail: ziyu.liu@sdu.edu.cn*
[d] *Key Laboratory of Optic-electric Sensing and Analytical Chemistry for Life Science, MOE, Qingdao University of Science and Technology, 266061 Qingdao, China*
† Electronic supplementary information (ESI) available. See DOI: https://doi.org/10.1039/d3nr00488k

SAzyme sensors were fabricated for continuously tracking the dynamic trends of AA in the human subject and also detecting AA content in nutritional products. Our work opens the door for the design of artificial single-atom catalysts to mimic natural enzymes and the development of corresponding biosensors.

Results and discussion

Synthesis and characterization of Rh SAzymes

The Rh SAzymes were synthesized *via* the well-developed host–guest strategy. Fig. 1a depicts the preparation process of Rh SAzymes. Zeolite imidazolate framework 8 (ZIF-8) was selected as the host, while Rh(acac)$_3$ acted as the guest, as its diameter (9.36 Å) falls in between the diameters of ZIF-8 pores (3.4 Å) and cavities (11.3 Å). Therefore, Rh(acac)$_3$ could be trapped within the molecular cages of ZIF-8 during crystallization. After being pyrolyzed at high temperatures, Rh atoms could be anchored *in situ* onto nitrogen-doped carbon derived from ZIFs. Inductively coupled plasma optical emission spectroscopy (ICP-OES) revealed a Rh loading of about 1 wt% for the as-synthesized Rh SAzymes.

The morphology of the as-synthesized Rh SAzymes was characterized by scanning electron microscopy (SEM) and transmission electron microscopy (TEM). As shown in Fig. 1b and c, the Rh SAzymes retain a dodecahedral shape with a uniform diameter of about 400 nm. Energy-dispersive X-ray spectroscopy (EDS) maps (Fig. 1d) demonstrate the homo-geneous distribution of C, N, Zn, and Rh elements throughout the entire architecture. As shown in Fig. 1e, the aberration-corrected high-angle annular dark-field scanning transmission electron microscopy (HAADF-STEM) image displays numerous bright dots with sub-angstrom size, further confirming the construction of isolated Rh single-atom sites (part of them is marked by circles). Moreover, no obvious Rh nanoparticles or clusters were detected. The XRD pattern of the as-obtained Rh SAzymes shows two broad diffraction peaks at 24° and 43° (Fig. S1†), which can be indexed to the (002) and (101) planes of N-doped graphitic carbon, respectively. Notably, no peaks related to metallic Rh or other Rh species has been observed, which is consistent with the HADDF-STEM results.

To elucidate the atomic structure of Rh SAzymes, X-ray absorption spectroscopy (XAS) was further employed. Fig. 1f shows the X-ray absorption near edge structure (XANES) of the Rh k-edge region. Ru metal foil and RuCl$_3$ powder were measured as a reference. The XANES spectrum is strongly influenced by the local electronic structure and configuration around the absorbing atom. The oxidation state of the central metal atom can be determined by its edge position. As shown in Fig. 1f, the absorption edge position of Rh is comparable to that of RhCl$_3$, indicating that the Rh valence state is close to +3. The local coordination environment of Rh is further investigated by the extended X-ray absorption fine structure (EXAFS) analysis. EXAFS oscillations of the Ru k-edge from Rh SAzymes, Rh foil, and RhCl$_3$ in k spaces are shown in Fig. S2.† As shown in Fig. 1g, the Fourier transform (FT) EXAFS spectra show a distinct peak at about 1.5 Å for the as-obtained Rh SAzymes, which could be attributed to the Rh–N/O coordi-nation shell. Meanwhile, the Rh–Rh coordination shell peak at about 2.4 Å is not detected, further proving the construction of isolated Rh sites in our Rh SAzymes. A combination of XRD, TEM, and HAADF-STEM analyses revealed that the single-atom Rh active sites have been successfully achieved.

Electrocatalytic AA oxidation

The electrochemical oxidation of AA involves a two-electron, two-proton transfer process, yielding dehydroascorbic acid (DHAA) as the product.[38,39] The oxidation process therefore may follow two types of mechanisms: (i) a stepwise mecha-nism, where electron transfers occur sequentially followed by bond formation, and/or (ii) a concerted mechanism, where both electron transfer and bond formation occur simul-taneously. The electrochemical transfer coefficient (β) is shown to be a sensitive probe of the mechanism by which electron transfer and bond cleavage may be coupled in dissociative electron transfer.[40] The charge transfer coefficient of an irre-versible electron transfer process is related to activation free energy ($\Delta G(E)$) and reaction free energy (ΔG^o). Combining with Butler Volmer's equation, the transfer coefficient is related to the peak potential and peak width ($\Delta E_{p/2}$) as in the following equation:

$$\beta = \frac{\Delta G(E)}{\Delta G^o} = \frac{\Delta G(E)}{F(E - E^o)} = \frac{1.86RT}{F|E_p - E_{p/2}|} \quad (1)$$
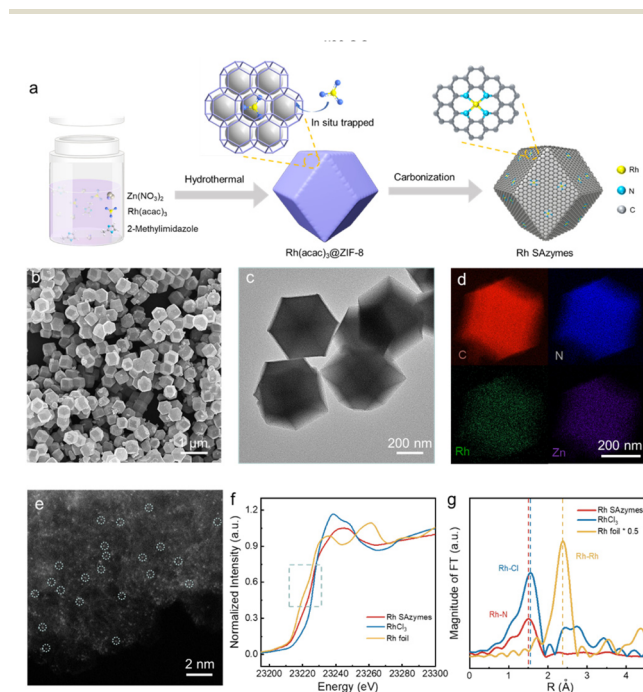
Fig. 1 The design and characterization of Rh SAzymes. (a) Schematic illustration of the preparation process. (b) SEM image, (c) TEM image, (d) EDS element maps, and (e) aberration-corrected HAADF–STEM image of the Rh SAzymes. (f) XANES and (g) EXAFS spectra of the Rh SAzymes, RhCl$_3$, and Rh foil at the Rh k-edge.

The above theoretical approaches can be adjusted for investigating the oxidation mechanism occurring at the Rh SAzymes. Fig. 2a presents the electrochemical redox behaviors at different scan rates in the presence of 10 mM AA. The corresponding β values at different scan rates are estimated as shown in Fig. 2b. As a result, the β remains nearly constant regardless of the applied scan rate, indicating the irreversible oxidation reaction. As well-demonstrated previously,[40,41] a charge transfer coefficient higher than 0.5 corresponds to a stepwise oxidation mechanism. Thus, the electrocatalytic oxidation reaction of AA proceeds stepwise, which is schematically illustrated in the inset of Fig. 2b. The first step is deprotonation leading to deprotonated AA molecules (intermediate a) with usually fast kinetics, which further convert into intermediate b by losing an electron. Subsequently, it transforms into intermediate c *via* further deprotonation. Eventually, the intermediate c is oxidized to DHAA by releasing another electron.

To further explore the importance of single-atomic coordination of Rh SAzymes, Rh-based nanocrystals were chosen for comparisons. The Rh and RhO$_x$ nanocrystals were prepared according to the literature[51] and further dispersed on carbon for following explorations (*i.e.*, Rh/C and RhO$_x$/C). Rh/C exhibits a uniform porous and dendritic morphology with an average diameter of 70 nm (Fig. S3†). The corresponding XRD pattern (Fig. S4†) further confirms the successful synthesis of metallic Rh.[51] The as-obtained Rh/C was calcined in air to obtain the oxidized form of RhO$_x$, which retains a similar morphology indicated by TEM characterization (Fig. S5†). The electrocatalytic oxidation of AA upon Rh SAzymes, RhO$_x$/C, and Rh/C were evaluated by cyclic voltammetry (CV) in 0.1 M PBS solution. Fig. 2c shows the background-corrected CV curves, among which the peaks at ~0.02 V can be ascribed to the oxidation of AA to DHAA. Surprisingly, the Rh SAzymes exhibit a peak current of 170 μA, which is much higher than those of RhO$_x$/C and Rh/C (Fig. 2d). The electrocatalytic per-

formance of Rh SAzymes was further compared with those of Pd/C and Pt/C which have been widely used as benchmark catalysts (Fig. S9†). The results reveal that Rh SAzymes exhibit superior current density and onset potential. Although the AA oxidation reaction is a reversible two-electron process, the oxidation of ascorbate is accompanied by a rapid hydration reaction, thus leading to a hardly detectable cathodic peak for this redox process.[52] It should be noted that the small peaks that appear before AA oxidation are assigned to the oxidation of Rh species.[53] To diminish the effect of Rh loading, the peak currents were normalized by Rh mass. The resultant mass activity is given in Fig. 2d, in which the value of Rh SAzymes is about 13 and 19 times higher than those of RhO$_x$/C and Rh/C, respectively. Furthermore, the anodic peak potential of Rh SAzymes is 0.02 V which is much lower than those of the recently reported catalysts, as shown in Fig. 2e, further demonstrating the promising electrocatalytic activity of Rh SAzymes.[42–50]

Design of miniaturized AA sensors

The high electrocatalytic activity of Rh SAzymes for AA oxidation endows them with great potential toward high-performance sensors. As shown in Fig. 3a and b, a portable AA sensing platform has been developed by using Rh SAzymes as the electrocatalysts. Working, counter, and reference electrodes are screen-printed with an insulating layer to be coated afterward. The printed electrodes exhibit well-defined redox peaks of ferricyanide ions with a reduction–oxidation potential difference of 86 mV (Fig. S6†), indicating a fast rate of heterogeneous electron transfer. The drop-casting of a Rh SAzyme catalyst layer was followed by that of a permeable Nafion layer for immobilization and to prevent possible interferences. By corre-
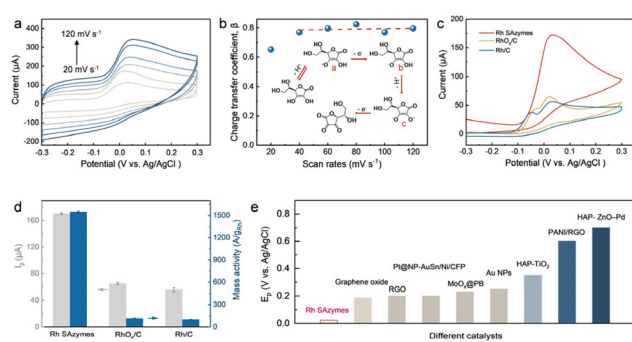
Fig. 2 Electrocatalytic oxidation of AA. (a) CVs of Rh SAzymes in 10 mM AA and 0.1 M PBS at different scan rates (20, 40, 60, 80, 100, and 120 mV s⁻¹) and (b) the corresponding β *versus* scan rate. (c) Background-corrected CV curves of Rh SAzymes, RhO$_x$/C, and Rh/C at a scan rate of 50 mV s⁻¹ in 10 mM AA and 0.1 M PBS. (d) The corresponding peak currents and mass activities of Rh SAzymes, RhO$_x$/C, and Rh/C for AA oxidation. (e) Comparison of the anodic peak potential for Rh SAzymes and previously reported catalysts.[42–50]
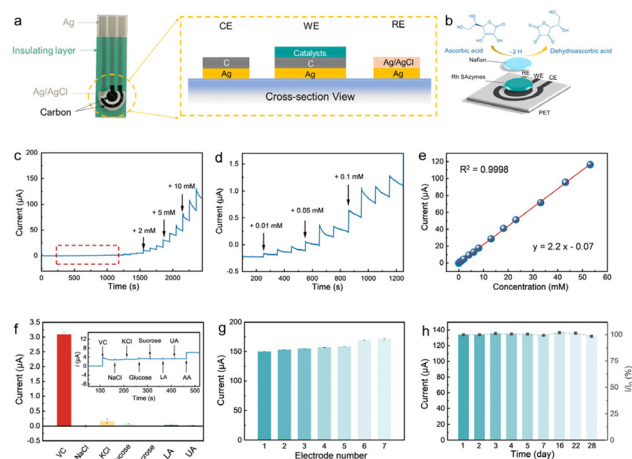
Fig. 3 Miniaturized electrochemical sensor. (a) The optical image and cross-section view of a screen-printed sensor. (b) Scheme of the modified working electrode. (c) Amperometric responses of the Rh SAzyme sensor to the successive addition of AA, and (d) a zoomed-in area of the red square region. (e) The corresponding concentration–current fitted curve. (f) The selectivity, (g) reproducibility and (h) stability tests of the Rh SAzyme sensor.

lating the peak currents (I_p) and the square root of the scan rates (Fig. S7†), the as-obtained sensor demonstrates similar diffusion-controlled reaction kinetics.

Owing to the excellent electrocatalytic activity of Rh SAzymes, an amperometric AA sensor has been developed. The sensing capability of the as-obtained sensor was demonstrated by a linear relationship between the current response and AA concentration for a large range of 2 to 20 mM (Fig. S8†). Furthermore, chronoamperometry tests were carried out to evaluate the linear range and sensitivity of Rh SAzymes in 0.1 M PBS solution. As shown in Fig. 3c and d, the current response steadily increases with the continuous addition of AA. Fig. 3d shows the excellent amperometric signals for the low concentration region. Further numerical fitting in Fig. 3e yielded a wide linear response range from 10.0 μM to 53.09 mM with excellent linearity (R^2 = 0.9998). Notably, the linear range of the Rh SAzyme sensor for AA detection surpasses those of most of the reported non-enzymatic sensors (Table S1†), highlighting an excellent potential for practical applications. The corresponding sensitivity is calculated to be 31.42 μA mM^{-1} cm^{-2} after the slope of the calibration curve was divided by the geometrical area of the working electrode. The detection limit was estimated as 0.26 μM, which is much lower than the median salivary AA levels of healthy humans (about 90 μM).[54]

The anti-interference performance was assessed by comparing the current response of the Rh SAzyme sensor to AA in the presence of common possible interfering chemicals, including NaCl, KCl, glucose, sucrose, lactic acid, and uric acid (Fig. 3f). The as-obtained sensor shows a significant signal to 1.5 mM AA, whereas the interference response ratio is less than 4.96%. Such good selectivity of this AA sensor is ascribed to the uniform structure of the Rh active sites, ensuring the accurate detection of the target in the complex physiological environment. The reproducibility was evaluated by the I_{pa} of 10 mM AA in 0.1 M PBS with seven identical working electrodes modified by the same method. Excitingly, the relative standard deviation (RSD) values were calculated to be less than 5% (Fig. 3g), demonstrating the high repeatability of the Rh SAzyme sensor. Moreover, the long-term stability of the Rh SAzyme sensor was also evaluated over a period of 28 days, and it exhibited nearly constant signal responses with a standard deviation of 1.05% (Fig. 3h).

Practical applications

The practical application of the Rh SAzyme sensors was further evaluated by direct monitoring of the dynamic changes of AA from saliva. The i–t curves for artificial saliva[55] (Table S2†) containing various concentrations of AA were analyzed by dropping the sample directly on the sensor (Fig. 4a). Fig. 4b gives the linear fit of the current response and AA concentration, in which the adjusted R-squared value is 0.997, indicating the accuracy and the potential for practical applications. Furthermore, we evaluated the temporal profile of saliva AA by measuring the response in a healthy human subject every 20 min after the intake of AA pills. The collected
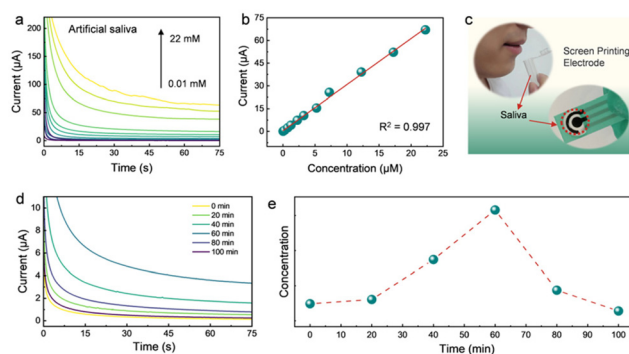
Fig. 4 Analysis of AA in personalized saliva. (a) Responses of the Rh SAzyme sensor to different concentrations of AA in artificial saliva, and (b) the corresponding concentration–current fitted curve. (c) Schematic diagram of the analysis of saliva samples with the Rh SAzyme sensor. (d) Response of a Rh SAzyme sensor to AA in saliva before and after taking 1 g AA pills at 20 min intervals. (e) The corresponding signal response vs. time.

saliva was used directly without further treatment (Fig. 4c). The change in the saliva AA signal was estimated by measuring the difference between the signal after taking the vitamin pill and the initial baseline recorded before taking the vitamin pill. The amperometric response of saliva AA at 0, 20, 40, 60, 80, and 100 min after taking the 1 g AA pill is shown in Fig. 4d. The maximum AA signal is achieved at 60 min after taking the vitamin supplement, followed by a decrease back to the baseline after 100 min. The corresponding saliva AA temporal profile, shown in Fig. 4e, reflects the pharmacokinetic profile of AA as described in previous studies.[9,56]

The Rh SAzyme sensor has broader applicability due to its wide linear detection range and high selectivity. The as-obtained Rh SAzyme sensors were applied to a rapid determination of AA levels in nutritional products (Fig. 5a). The composition of the different oral formulations of nutritional pro-
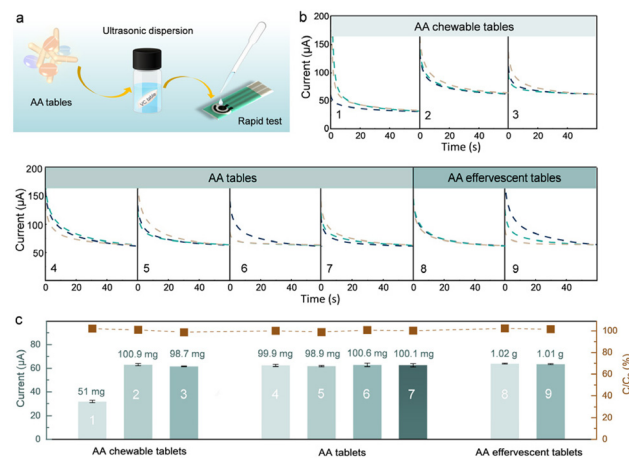
Fig. 5 Analysis of AA in nutritional products. (a) Illustration of the Rh SAzyme sensor for onsite detection of AA in nutritional products. (b) Response of the Rh SAzyme sensor to various types of AA products. (c) Test results and comparison with theoretical values.

ducts is given in Table S3.† The amperometric method was used to determine the concentration of AA in a diluted PBS solution. The current curves of nine different nutrition products are shown in Fig. 5b, based on which the AA contents were calculated and are listed in Fig. 5c. The results from our Rh SAzyme sensor agree well with the indicated contents of the products within 3% deviation. Compared to conventional vitamin monitoring techniques, such as liquid chromatography, our Rh SAzyme sensing platform exhibits excellent convenience, cost control, and reliability for detecting AA levels in nutritional products.

Conclusion

In this work, single-atom Rh active sites were constructed to mimic ascorbate peroxidase, which exhibits an unprecedented electrocatalytic activity toward AA oxidation with an onset potential of 0.02 V. The Rh SAzyme-based sensor achieves an excellent AA detection performance with a very wide linear range of 10.0 μM–53.1 mM, a low detection limit of 0.26 μM and a long stability of more than 28 days, as well as desirable sensitivity (31.42 μA mM^{-1} cm^{-2}) and reproducibility. Moreover, the miniaturized sensor exhibits a broader application potential for rapid analysis of AA levels in nutritional products. Our work presents a vivid example of designing artificial single-atom catalysts to mimic natural enzymes and suggests the potential to develop next-generation electrochemical biosensors based on single-atom nanozymes.

Data availability

All experimental procedures and characterization data that support the findings of this study are available in the main text and ESI.†

Conflicts of interest

There are no conflicts to declare.

Acknowledgements

References

1 M. Levine, J. S. Flier and J. B. Young, New concepts in the biology and biochemistry of ascorbic-acid, *N. Engl. J. Med.*, 1986, **314**, 892–902.

2 A. C. Carr and S. Rowe, The emerging role of vitamin c in the prevention and treatment of covid-19, *Nutrients*, 2020, **12**, 1–8.

3 N. Shenoy, E. Creagan, T. Witzig and M. Levine, Ascorbic acid in cancer treatment: Let the phoenix fly, *Cancer Cell*, 2018, **34**, 700–706.

4 W. Zhang, L. Liu, Y. Li, D. Wang, H. Ma, H. Ren, Y. Shi, Y. Han and B.-C. Ye, Electrochemical sensing platform based on the biomass-derived microporous carbons for simultaneous determination of ascorbic acid, dopamine, and uric acid, *Biosens. Bioelectron.*, 2018, **121**, 96–103.

5 Y. Yu, H. Y. Y. Nyein, W. Gao and A. Javey, Flexible electrochemical bioelectronics: The rise of in situ bioanalysis, *Adv. Mater.*, 2020, **32**, 1–25.

6 J. R. Sempionatto, V. R.-V. Montiel, E. Vargas, H. Teymourian and J. Wang, Wearable and mobile sensors for personalized nutrition, *ACS Sens.*, 2021, **6**, 1745–1760.

7 G. Li, J. Hao, W. Li, F. Ma, T. Ma, W. Gao, Y. Yu and D. Wen, Integrating highly porous and flexible au hydrogels with soft-mems technologies for high-performance wearable biosensing, *Anal. Chem.*, 2021, **93**, 14068–14075.

8 L. Chen, F. Chen, G. Liu, H. Lin, Y. Bao, D. Han, W. Wang, Y. Ma, B. Zhang and L. Niu, Superhydrophobic functionalized ti3c2tx mxene-based skin-attachable and wearable electrochemical ph sensor for real-time sweat detection, *Anal. Chem.*, 2022, **94**, 7319–7328.

9 J. R. Sempionatto, A. A. Khorshed, A. Ahmed, E. S. A. N. De Loyola, A. Barfidokht, L. Yin, K. Y. Goud, M. A. Mohamed, E. Bailey, J. May, C. Aebischer, C. Chatelle and J. Wang, Epidermal enzymatic biosensors for sweat vitamin c: Toward personalized nutrition, *ACS Sens.*, 2020, **5**, 1804–1813.

10 J. R. Sempionatto, L. C. Brazaca, L. Garcia-Carmona, G. Bolat, A. S. Campbell, A. Martin, G. Tang, R. Shah, R. K. Mishra, J. Kim, V. Zucolotto, A. Escarpa and J. Wang, Eyeglasses-based tear biosensing system: Non-invasive detection of alcohol, vitamins and glucose, *Biosens. Bioelectron.*, 2019, **137**, 161–170.

11 J. R. Sempionatto, V. R. Montiel, E. Vargas, H. Teymourian and J. Wang, Wearable and mobile sensors for personalized nutrition, *ACS Sens.*, 2021, **6**, 1745–1760.

12 K. A. Naidu, Vitamin c in human health and disease is still a mystery ? An overview, *Nutr. J.*, 2003, **2**, 1–10.

13 L. Jiao, H. Yan, Y. Wu, W. Gu, C. Zhu, D. Du and Y. Lin, When nanozymes meet single-atom catalysis, *Angew. Chem., Int. Ed.*, 2020, **59**, 2565–2576.

14 S. Ji, B. Jiang, H. Hao, Y. Chen, J. Dong, Y. Mao, Z. Zhang, R. Gao, W. Chen, R. Zhang, Q. Liang, H. Li, S. Liu, Y. Wang, Q. Zhang, L. Gu, D. Duan, M. Liang, D. Wang, X. Yan and Y. Li, Matching the kinetics of natural enzymes with a single-atom iron nanozyme, *Nat. Catal.*, 2021, **4**, 407–417.

15 Z. Zhang, J. Zhu, S. Chen, W. Sun and D. Wang, Liquid fluxional ga single atom catalysts for efficient electrochemical co2 reduction, *Angew. Chem., Int. Ed.*, 2023, DOI: **10.1002/anie.202215136**.

16 X.-F. Cheng, J.-H. He, H.-Q. Ji, H.-Y. Zhang, Q. Cao, W.-J. Sun, C.-L. Yan and J.-M. Lu, Coordination symmetry breaking of single-atom catalysts for robust and efficient nitrate electroreduction to ammonia, *Adv. Mater.*, 2022, **34**, 1–10.

17 Z.-Y. Wu, M. Karamad, X. Yong, Q. Huang, D. A. Cullen, P. Zhu, C. Xia, Q. Xiao, M. Shakouri, F.-Y. Chen, J. Y. Kim, Y. Xia, K. Heck, Y. Hu, M. S. Wong, Q. Li, I. Gates, S. Siahrostami and H. Wang, Electrochemical ammonia synthesis via nitrate reduction on fe single atom catalyst, *Nat. Commun.*, 2021, **12**, 1–10.

18 S. Lin and H. Wei, Design of high performance nanozymes: A single-atom strategy, *Sci. China: Life Sci.*, 2019, **62**, 710–712.

19 H. Wei, L. Gao, K. Fan, J. Liu, J. He, X. Qu, S. Dong, E. Wang and X. Yan, Nanozymes: A clear definition with fuzzy edges, *Nano Today*, 2021, **40**, 1–6.

20 B. Jiang and M. Liang, Advances in single-atom nanozymes research, *Chin. J. Chem.*, 2021, **39**, 174–180.

21 J. Wu, X. Wang, Q. Wang, Z. Lou, S. Li, Y. Zhu, L. Qin and H. Wei, Nanomaterials with enzyme-like characteristics (nanozymes): Next-generation artificial enzymes (ii), *Chem. Soc. Rev.*, 2019, **48**, 1004–1076.

22 J. Yang, W. H. Li, K. Xu, S. Tan, D. Wang and Y. Li, Regulating the tip effect on single-atom and cluster catalysts: Forming reversible oxygen species with high efficiency in chlorine evolution reaction, *Angew. Chem., Int. Ed.*, 2022, **61**, 1–8.

23 Y. Xiong, W. Sun, Y. Han, P. Xin, X. Zheng, W. Yan, J. Dong, J. Zhang, D. Wang and Y. Li, Cobalt single atom site catalysts with ultrahigh metal loading for enhanced aerobic oxidation of ethylbenzene, *Nano Res.*, 2021, **14**, 2418–2423.

24 Y. Wang, X. Zheng and D. Wang, Design concept for electrocatalysts, *Nano Res.*, 2022, **15**, 1730–1752.

25 R. Li and D. Wang, Understanding the structure-performance relationship of active sites at atomic scale, *Nano Res.*, 2022, **15**, 6888–6923.

26 M. Liu, N. Li, S. Cao, X. Wang, X. Lu, L. Kong, Y. Xu and X.-H. Bu, A "pre-constrained metal twins" strategy to prepare efficient dual-metal-atom catalysts for cooperative oxygen electrocatalysis, *Adv. Mater.*, 2022, **34**, 1–9.

27 Y. Wang, R. Shi, L. Shang, G. I. N. Waterhouse, J. Zhao, Q. Zhang, L. Gu and T. Zhang, High-efficiency oxygen reduction to hydrogen peroxide catalyzed by nickel single-atom catalysts with tetradentate n2 o2 coordination in a three-phase flow cell, *Angew. Chem., Int. Ed.*, 2020, **59**, 13057–13062.

28 Z. Liu, Y. Du, R. Yu, M. Zheng, R. Hu, J. Wu, Y. Xia, Z. Zhuang and D. Wang, Tuning mass transport in electrocatalysis down to sub-5 nm through nanoscale grade separation, *Angew. Chem., Int. Ed.*, 2023, DOI: **10.1002/anie.202212653**.

29 P. Zhu, X. Xiong and D. Wang, Regulations of active moiety in single atom catalysts for electrochemical hydrogen evolution reaction, *Nano Res.*, 2022, **15**, 5792–5815.

30 G. Wang, C. T. He, R. Huang, J. Mao, D. Wang and Y. Li, Photoinduction of cu single atoms decorated on uio-66-nh2 for enhanced photocatalytic reduction of co2 to liquid fuels, *J. Am. Chem. Soc.*, 2020, **142**, 19339–19345.

31 Y. Yao, L. Zhao, J. Dai, J. Wang, C. Fang, G. Zhan, Q. Zheng, W. Hou and L. Zhang, Single atom ru monolithic electrode for efficient chlorine evolution and nitrate reduction, *Angew. Chem., Int. Ed.*, 2022, **61**, 1–7.

32 B. Long, Y. Zhao, P. Cao, W. Wei, Y. Mo, J. Liu, C.-J. Sun, X. Guo, C. Shan and M.-H. Zeng, Single-atom pt boosting electrochemical nonenzymatic glucose sensing on ni(oh)2/n-doped graphene, *Anal. Chem.*, 2022, **94**, 1919–1924.

33 W. Zhou, Y. Tan, J. Ma, X. Wang, L. Yang, Z. Li, C. Liu, H. Wu, L. Sun and W. Deng, Ultrasensitive no sensor based on a nickel single-atom electrocatalyst for preliminary screening of covid-19, *ACS Sens.*, 2022, **7**, 3422–3429.

34 X. Xie, D. P. Wang, C. Guo, Y. Liu, Q. Rao, F. Lou, Q. Li, Y. Dong, Q. Li, H. B. Yang and F. X. Hu, Single-atom ruthenium biomimetic enzyme for simultaneous electrochemical detection of dopamine and uric acid, *Anal. Chem.*, 2021, **93**, 4916–4923.

35 K. H. Sharp, M. Mewies, P. C. Moody and E. L. Raven, Crystal structure of the ascorbate peroxidase-ascorbate complex, *Nat. Struct. Biol.*, 2003, **10**, 303–307.

36 A. P. Ledray, C. M. Krest, T. H. Yosca, K. Mittra and M. T. Green, Ascorbate peroxidase compound ii is an iron (iv) oxo species, *J. Am. Chem. Soc.*, 2020, **142**, 20419–20425.

37 S. J. Thompson, M. R. Brennan, S. Y. Lee and G. Dong, Synthesis and applications of rhodium porphyrin complexes, *Chem. Soc. Rev.*, 2018, **47**, 929–981.

38 M. M. Hasan, R. H. Rakib, M. Abul Hasnat and Y. Nagao, Electroless deposition of silver dendrite nanostructure onto glassy carbon electrode and its electrocatalytic activity for ascorbic acid oxidation, *ACS Appl. Energy Mater.*, 2020, **3**, 2907–2915.

39 I. F. Hu and T. Kuwana, Oxidative mechanism of ascorbic-acid at glassy-carbon electrodes, *Anal. Chem.*, 1986, **58**, 3235–3239.

40 S. Antonello and F. Maran, The role and relevance of the transfer coefficient alpha in the study of dissociative electron transfers: Concepts and examples from the electroreduction of perbenzoates, *J. Am. Chem. Soc.*, 1999, **121**, 9668–9676.

41 M. A. Hasnat, M. M. Hasan, N. Tanjila, M. M. Alam and M. M. Rahman, Ph dependent kinetic insights of electro-

catalytic arsenite oxidation reactions at pt surface, *Electrochim. Acta*, 2017, **225**, 105–113.

42 H. Yang, J. Zhao, M. Qiu, P. Sun, D. Han, L. Niu and G. Cui, Hierarchical bi-continuous pt decorated nanoporous au-sn alloy on carbon fiber paper for ascorbic acid, dopamine and uric acid simultaneous sensing, *Biosens. Bioelectron.*, 2019, **124**, 191–198.

43 G. Veerapandi, S. Meenakshi, S. Anitta, C. Arul, P. Ashokkumar and C. Sekar, Precise and quick detection of ascorbic acid and eugenol in fruits, pharmaceuticals and medicinal herbs using hydroxyapatite-titanium dioxide nanocomposite-based electrode, *Food Chem.*, 2022, **382**, 132251–132251.

44 J. Ma, L. Shen, Y. Jiang, H. Ma, F. Lv, J. Liu, Y. Su and N. Zhu, Wearable self-powered smart sensors for portable nutrition monitoring, *Anal. Chem.*, 2022, **94**, 2333–2340.

45 F. Bettazzi, C. Ingrosso, P. S. Sfragano, V. Pifferi, L. Falciola, M. L. Curri and I. Palchetti, Gold nanoparticles modified graphene platforms for highly sensitive electrochemical detection of vitamin c in infant food and formulae, *Food Chem.*, 2021, **344**, 1–8.

46 L. V. de Faria, T. P. Lisboa, D. M. de Farias, F. M. Araujo, M. M. Machado, R. A. de Sousa, M. A. Costa Matos, R. A. Abarza Munoz and R. C. Matos, Direct analysis of ascorbic acid in food beverage samples by flow injection analysis using reduced graphene oxide sensor, *Food Chem.*, 2020, **319**, 1–6.

47 L. Yu, J. Zhao, S. Tricard, Q. Wang and J. Fang, Efficient detection of ascorbic acid utilizing molybdenum oxide@-prussian blue/graphite felt composite electrodes, *Electrochim. Acta*, 2019, **322**, 1–11.

48 S. A. Shahamirifard and M. Ghaedi, A new electrochemical sensor for simultaneous determination of arbutin and vitamin c based on hydroxyapatite-zno-pd nanoparticles modified carbon paste electrode, *Biosens. Bioelectron.*, 2019, **141**, 111474.

49 L. Huang, Y. Cao and D. Diao, Surface n-doped graphene sheets induced high electrocatalytic activity for selective ascorbic acid sensing, *Sens. Actuators, B*, 2019, **283**, 556–562.

50 H. Karimi-Maleh and O. A. Arotiba, Simultaneous determination of cholesterol, ascorbic acid and uric acid as three essential biological compounds at a carbon paste electrode modified with copper oxide decorated reduced graphene oxide nanocomposite and ionic liquid, *J. Colloid Interface Sci.*, 2020, **560**, 208–212.

51 W. Wang, Z. Cao, K. Liu, J. Chen, Y. Wang and S. Xie, Ligand-assisted, one-pot synthesis of rh-on-cu nanoscale sea urchins with high-density interfaces for boosting co oxidation, *Nano Lett.*, 2017, **17**, 7613–7619.

52 M. R. Deakin, P. M. Kovach, K. J. Stutts and R. M. Wightman, Heterogeneous mechanisms of the oxidation of catechols and ascorbic-acid at carbon electrodes, *Anal. Chem.*, 1986, **58**, 1474–1480.

53 M. Rajkumar, S. Thiagarajan and S.-M. Chen, Electrochemical fabrication of rh–pd particles and electrocatalytic applications, *J. Appl. Electrochem.*, 2011, **41**, 663–668.

54 G. Isola, A. Polizzi, S. Muraglie, R. Leonardi and A. Lo Giudice, Assessment of vitamin c and antioxidant profiles in saliva and serum in patients with periodontitis and ischemic heart disease, *Nutrients*, 2019, **11**, 1–13.

55 J. Y. Gal, Y. Fovet and M. Adib-Yadzi, About a synthetic saliva for in vitro studies, *Talanta*, 2001, **53**, 1103–1115.

56 S. Hickey, H. J. Roberts and N. J. Miller, Pharmacokinetics of oral vitamin c, *J. Nutr. Environ. Med.*, 2009, **17**, 169–177.